Gas-dynamic and electro-chemical optimization of catalyst layers in high temperature polymeric electrolyte membrane fuel cells

Gas-dynamic and electro-chemical optimization of catalyst layers in high temperature polymeric electrolyte membrane fuel cells

Uktam R. Salomov[1], Eliodoro Chiavazzo[1], Pietro Asinari[1,*]

multi-Scale ModeLing Laboratory (SMaLL), Dipartimento Energia, Politecnico di Torino, Corso Duca degli Abruzzi 24, Zip code 10129, Torino, ITALY

Abstract

We investigate the impact of catalyst (Pt) particle distribution on gas dynamics, electro-chemistry and consequently the performance of high temperature polymeric electrolyte membrane (HTPEM) fuel cells. We demonstrate that optimal distribution of catalyst can be used as an effective mitigation strategy for phosphoric acid loss and crossover of reagents through the membrane. We recognize that one of the reasons of degradation of HTPEM fuel cell performance is the gas dynamic pulling stress at the interface between the catalyst layer and the membrane. This stress, though, can be highly reduced. We have performed direct numerical pore-scale simulations of the gas flow through the catalyst layer for different distributions of catalyst particles, in order to minimize this stress and hence to improve durability. The results of pore-scale simulation for exponential decay distribution show over one

*Corresponding author

Email addresses: uktam.salomov@polito.it (Uktam R. Salomov), eliodoro.chiavazzo@polito.it (Eliodoro Chiavazzo), pietro.asinari@polito.it (Pietro Asinari)

URL: http://staff.polito.it/pietro.asinari/ (Pietro Asinari), http://www.polito.it/small (Pietro Asinari)

order of magnitude reduction of the pulling stress, compared to the homogeneous (conventional) distribution. In addition, a simplified three-dimensional macroscopic model of the membrane electrode assembly with catalyst layer made of three sub-layers with different catalyst loadings, has been developed. The latter model predicts 67% reduction in pulling stress using a feasible mitigation strategy, at the cost of only 9.3% efficiency reduction at high current densities.
Keywords: High temperature PEM fuel cells, Degradation, Catalyst distribution, Fuel cell performance, Electro-chemical modeling

---

Contents

1. Introduction

Fuel cells have been the subject of a large amount of research owing to the fact that are considered an environmentally friendly and clean energy source. In particular, proton exchange membrane fuel cells (PEMFC) have attracted much attention due to a wide range of possible applications including small-scale power sources, car propulsion, domestic use and supply of portable devices. A next generation of PEMFCs at high temperature (above 100 ^{o}C) has been introduced to address the issues of the low temperature (LT) counterpart, by system simplification, reduction of the production cost, and improvement of the efficiency [2, 3, 4]. As a result, high tolerance of platinum based catalyst to fuel CO impurity (up to 2% at 180^{o}C in the absence of humidification [5, 6]) has been achieved for the high temperature (HT) PEMFCs. Moreover, chemically coupled with acids membranes (polymer electrolyte) show enhanced ionic conductivity [7].

To this end, significant amount of investigations on phosphoric-acid (PA)-doped polybenzimidazole(PBI)-based HT-PEMFCs membranes have been carried out with regards to the membrane conductivity and heat resistance [8, 9]. In [10, 11], authors addressed the issue of power generation capability. It was found that the highest fuel cell performance can be obtained at the operating temperature close to 200 ^{o}C [12]. Durability exceeding ten thousand hours has been reported by several research groups [13, 14], which might be considered a suitable requirement for commercialization.

One of the main issues limiting the widespread adoption and successful commercialization of polymer-electrolyte fuel cells, especially for automotive applications, are those of lifetime or durability, under various operating

conditions, and cost. Although the number of installed units continues to increase and dominates the pre-markets worldwide, the present lifetime requirements for fuel cells cannot be guaranteed. This certainly stimulates research for a more comprehensive knowledge of the material aging mechanisms.

A more advanced knowledge of the mechanisms leading to reversible or irreversible loss of cell performance, and the impact of the operating conditions on these mechanisms is highly desirable. This should be based on the observation of the changes in materials properties. The impact on fuel cell performance should be assessed, even before proceeding with optimization of materials, control systems and operating conditions. Modeling of different degradation aspects can help in highlighting the above stressed points by understanding the key reasons and fundamental physical phenomena underpinning particular degradation mechanisms, and thus predicting the impact of these degradation effects in advance. Another important aspect of modeling is the understanding of the interaction between different specific membrane degradation mechanisms and the overall (mixed) effects due to their simultaneous occurrence in real fuel cell operation. This requires a multi-scale description of the several phenomena involved, and it has motivated several recent studies on PEMFC degradation based on data of both long-term and rapid aging testing. It should be noted that modeling has been restricted mainly to the low-temperature PEMFC. However these investigations are of great interest also for high temperature PEMFCs, due to the fact that many degradation mechanisms are actually inherited from the low temperature counterpart [15].

Although, all components of hydrogen fuel cells are subject to degradation processes, the membrane electrode assembly (MEA) is commonly considered as the heart of the system and the most vulnerable element. Generally, MEAs consist of i) gas diffusive layers (GDL); ii) catalyst layers (CL) and iii) a membrane. The degradation of the noble metal catalysts within MEAs at the so-called three-phase-boundary (TPB) is an important phenomenon directly affecting the durability of the fuel cells [16, 17, 18]. There are two main degradation modes related to the membrane, namely (a) membrane thinning possibly leading to pinhole formation and (b) increased fuel crossover with loss of fuel efficiency by acid evaporation [19]. It was shown that phosphoric acid loss from the membrane is insignificant at 160 ^{o}C [19, 20]. Excessive compression of MEA causes membrane creep and thinning (manifested by gas crossover increase and decrease of the membrane resistance). Probably, the most extensively studied and modeled failure process is pinhole formation in membrane due to degradation caused by peroxide chemical attack [21, 22, 23]. There are two pathways for the generation of free radical species from hydrogen peroxide. Firstly, generation at the cathode due to the electrochemical two-electron reduction of oxygen [24], and secondly, generation at the anode owing to chemical combination of crossover oxygen and hydrogen [25, 26, 27]. Several groups [28, 29] worked to find a link between crossover of reagents and membrane degradation, where authors studied the effect of platinum on degradation of ionomer membranes in hydrogen/air mixtures, and a few stochastic degradation models have been proposed in Ref. [30] to predict the deterioration time evolution of different fuel cell properties, without considering much detail of the degradation modes. Some attempts have been made

to model the chemical degradation processes using a semi-empirical transient approach [28, 31]. The latter includes an equation for the residual ionomer mass within the cathode catalyst layer, which is treated as directly proportional to the rate of hydrogen crossover, and based on the assumption that radical species are produced at the cathode catalyst layer/membrane interface. Moreover, the thickness of the membrane is assumed to decrease as a linear function of the residual ionomer mass, and this has an impact on the calculation of the uniform hydrogen crossover flux. However, the influence of the operating conditions could not be accounted for in this simple model.

Among the several degradation mechanisms in high temperature MEA electrodes, the loss of catalyst metal (platinum) electrochemically active surface area (ECSA) by particle size growth is considered to play a major role. The phenomena underpinning this are thought to be:

i) Corrosion of carbon support leading to a loss of nanoparticle electrical contact [32];

ii) Particle migration and coalescence (leading to coarsening) [32, 33];

iii) Particle dissolution and off support re-precipitation (leading to mass loss);

iv) Particle dissolution and re-precipitation on support (leading to coarsening) [34].

It is also possible that coarsening may be caused by diffusion of platinum atoms to the carbon support.

Some effort has been dedicated to the modeling of the dissolution mechanism of platinum [35, 36] and to platinum migration using dilute solution equations. The mathematical description presented in Ref. [37] incorporates the kinetic expressions for platinum oxidation and dissolution into a transient, one-dimensional model of the cross section of a PEM fuel cell consisting of the following regions: anode gas-diffusion medium, anode catalyst layer, membrane, cathode catalyst layer, and cathode gas-diffusion medium. Porous-electrode theory is used to model the anode and cathode catalyst layers. The details of sintering, ripening and the reaction of platinum with hydrogen were ignored. Platinum ion transport by the bulk flow of liquid water was assumed to be negligible. A refinement of this model has been done in Ref. [38], where particle size distribution and crossover hydrogen are explicitly included. The oxidation model has been extensively modified, and a model for particle surface tension as a function of oxide coverage has been included.

In fact, the dissolution process of platinum particles is exacerbated or even initiated by another major degradation process during fuel cell operation, namely carbon support corrosion, which is a potential-dependent electrochemical process [39, 40, 41]. Corrosion of carbon support at the cathode catalyst results in electrical isolation of the catalyst particles, migration on the surface of the support material and agglomeration via Ostwald ripening mechanism [40]. Meanwhile, hydrophilicity of the cathodic catalyst layer is increased and accompanied by electrolyte flooding leading to an increase of the cathode mass transport overpotentials. The mass transport overpotential is responsible for diffusive transport of the reactants to the electrode surface

from bulk electrolyte and reverse transport of products. As a result, the oxygen reduction reaction kinetics decreases in the cathode. Concurrently to the corrosion of carbon, thinning of the catalyst layer and loss of its void volume can be observed [42]. In the worst case, complete degradation of the carbon support might even affect structural integrity of the cathode catalyst layer. Noticeable, carbon corrosion process depends not only on temperature and local potential, but also on water partial pressure [15, 40, 43].

Probably the first attempt of modeling this process has been done in [44], where a one-dimensional static model for the calculation of the potential profiles has been proposed with the anode partially exposed to air. Authors have proposed a reverse-current decay mechanism, where carbon corrosion occurs due to inadequate fuel quantities and possible crossover during startup and shutdown. A numerical finite element method is used for finding a solution of the Poisson equation coupled with a conservation equation of the electric charges and a classic Bulter-Volmer description of the global hydrogen oxidation reaction (HOR) and oxygen reduction reaction (ORR). Meyers and Darling [45] have proposed a similar model, which describes how a maldistribution of hydrogen across the fuel electrode can induce both oxygen permeation from the cathode to the anode and cathode carbon corrosion in the fuel starved region. Implications of this reverse current mechanism are explored by simulating a cell with a nonuniform distribution of hydrogen along the fuel channel in both steady-state and transient operation conditions. A one-dimensional (1D) mathematical model is used for taking into account the reactants transported in the channels and the Bulter-Volmer equations. It should be stressed that the above mentioned models describe how oper-

ating conditions affect carbon corrosion, although they are not adequate for predicting the impact of carbon corrosion on the instantaneous cell performance. Namely, the instantaneous feedback between performance and aging is not taken into account. Furthermore, the role of the catalyst in the carbon corrosion is not explored (platinum and carbon are treated as individual single phases). This issue has been partially addressed in Ref. [32]. Here, the proposed mechanistic model couples carbon corrosion with MEA electrocatalysis, which describes instantaneous cell performance. Additionally, the effect of operating conditions and catalyst layer parameters on lifetime of fuel cell have been estimated. Particularly, it was found that in the presence of oxygen in the anode compartment due to crossover or fuel starvation, the thickness of cathode catalyst layer decreases. One of the main results of this work is the existence of a maximal durability for a given external load.

In contrast to the above mentioned degradations, loss of phosphoric acid from membrane and electrodes is a peculiar degradation phenomenon of high temperature PBI-based phosphoric acid-doped PEMFC. The acidic environment of the fuel cell, combined with the humidity level and temperature, creates a harsh environment. Phosphoric acid (PA) losses are thought to play a major role in degradation, especially at high current density and elevated temperature ($> 160^o$C) [2], through different mechanisms, such as the ones mentioned below: capillary transport, diffusion, membrane compression, evaporation and leaching by condensed water during shutdown and cold start. Yu *et al.* [20] conducted steady-state operation tests (with constant current density $0.2\,A/cm^2$) and dynamic durability tests (load, thermal, and shutdown/start-up cycling tests, with operational conditions which may

be found in real applications) where the fuel cell potential and phosphoric acid loss were recorded over thousands of hours. It was found that higher acid loss rate is observed at the cathode side of MEA, due to the formation of liquid water, and a subsequent acid leaching. A significant increases in the PA loss rates and the voltage degradation were observed at elevated temperatures (180 and 190^{o}C) and high load conditions. It was concluded that degradation due to phosphoric acid loss appears to be a minor factor of fuel cell failure, compared to degradation caused by catalyst activity loss, during the first hours of continuous operation. However, after this first period, the platinum particles size tends to stabilize and the effect of phosphoric acid loss starts emerging [46].

A deeper insight into this degradation mechanism, leading to irreversible or reversible performance loss and the relation with other degradation mechanisms and the operating conditions, comes through pore-scale modeling of the mass transport phenomena, which is able to provide detailed information at microscopic level. The morphological model presented in [1] was developed as the first step towards an effort of simulating such degradation mechanisms (at a pore scale). This morphological model enables to extrapolate the specific results towards different materials. On the other hand, a morphological model correlates the transport coefficients with the global microscopic structure, but it also (a) explains how different features of the microscopic structure (characteristic lengths, distributions, shapes, orientations, clustering, etc.) determine independently the transport coefficients and (b) suggests design strategies to improve transport coefficients. Hence, a morphological model allows one to generate many virtual structures (all compatible with

the available experimental data) in order to find out a design strategy beyond experimental measurements. Here, we aim at extending further this model for enhancing our understanding on degradation phenomena.

Specifically, in this paper, we focus on the influence of a parameter in the above morphological model (i.e. the distribution of the catalyst platinum particles) on gas dynamics, electro-chemistry and consequently overall performance of high temperature proton exchange membrane (HT-PEM) fuel cells. Moreover, we suggest an optimal mass transport at the interface between the catalyst layers and the membrane and show how this strategy can be used to mitigate the issue of phosphoric acid loss and crossover of reagents through the membrane. The main idea behind the proposed mitigation strategy is a design of the optimal flow field through an appropriate distribution of the catalyst particles. Because the velocity gradient orthogonal to the interface is directly related to the pulling stress acting on the phosphoric acid inside the membrane, we force it to be equal to zero at the interface between the catalyst layer and the membrane. To this purpose, we have performed direct numerical simulations of the fluid flow through the catalyst layer for different distributions of catalyst particles. In addition, a three-dimensional model of the membrane electrode assembly (MEA) has been also developed to analyze how the proposed mitigation strategy affects the polarization curve and thus the cell performance.

The paper is organized as follows. In Section 2, a brief description of the adopted methodology, setups, geometrical configurations of both, pore-scale model of the flow through catalyst layer and macroscopic single MEA model, are presented. Section 3 describes the choice of the boundary conditions,

the idea behind PA loss mitigation, details and results of direct numerical simulations. Moreover, we report single MEA performance simulations for three different cases: homogeneous, exponentially decaying and exponentially increasing towards the membrane distributions. Conclusions and outlooks are reported in the final section.

2. Materials and methods

2.1. Three-dimensional pore-scale model of fluid flow through catalyst layer

In this section, we explore some catalyst layer (CL) configurations by tuning the distribution of the catalyst platinum (Pt) particles. In particular, we investigated the influence of Pt deposition inside catalyst layer on mass transport by performing pore-scale lattice Boltzmann simulations of the flow through the same porous medium, but with different distributions of catalyst particles.

Numerical fluid dynamics solvers based on the lattice Boltzmann method (LBM) are well established tools for coping with complex domains. The most popular LBM model for simulating flows in porous media is the one adopting the well known Bhatnagar-Gross-Krook (BGK) model in combination with a simple bounce-back scheme for at the solid-fluid interface [50]. All parameters used in the lattice Boltzmann method during the pore-scale modeling are presented in Table 1.

The main goal is to find an optimal configuration of the CL by probing different distributions of the catalyst particles. The catalyst particle distribution should be optimized in order to improve the performance of the PEMFCs and also to mitigate the degradation mechanisms (e.g. loss of

phosphoric acid). Such optimization can lead to a proper tuning of the mass transport properties of reactants (hydrogen, oxygen) and products (water, vapor) through the CL microstructure. For this, the morphological model proposed in Ref. [1] plays an essential role and it will be used here. It is important from the morphological point of view, to have small platinum particles ensuring large surface area finely dispersed on the catalyst support surface (typically, carbon powder).

It should be noted that the idea of considering a distribution of catalyst particles inside the CL has been already proposed in Ref. [1]. Conventional definition of permeability (where it is assumed that all catalyst particles are deposited at the interface between the catalyst layer and the membrane) does not rigorously apply to the CL, where electrochemical reactions happen inside the layer itself. In recent tomography data [47], it has been proven that catalyst particles are distributed inside CL quasi-homogeneously in most of the cases. We used the morphological model in [1] for reconstructing the microstructure of a carbon supported catalyst layer. Here, a one dimensional array $\mathcal{M}$ is used for describing the configuration, namely

$$\mathcal{M}_{i_x,i_y,i_z} = \begin{cases} 0 & (i_x, i_y, i_z) \in fluid \\ 1 & (i_x, i_y, i_z) \in fluid \bigcap solid \\ 2 & (i_x, i_y, i_z) \in solid \\ 3 & (i_x, i_y, i_z) \in catalyst\ particles \end{cases}$$

In order to fix ideas, let us consider two different configurations: homogeneous and exponential decay towards the polymeric membrane, as illustrated in Fig. 1. In the former homogeneous distribution, the probability to find catalyst particles remains constant in the entire CL, while in latter config-

uration it is lower and lower when moving towards the membrane. In this study, it is assumed that the catalyst particles are deposited on the surface of carbon support agglomerates. The catalyst layer has been equally divided into n_p number of parts in the $x-$direction (i.e. the main flow direction towards the membrane). To obtain quasi-homogeneous distribution of catalyst particles throughout the CL, a fixed number of bounce-back nodes ($\mathcal{M}_{i_x,i_y,i_z} = 1$) are randomly switched to catalyst nodes ($\mathcal{M}_{i_x,i_y,i_z} = 3$) in each CL sub-layer. Clearly, the total number of available catalyst nodes N_t equals the summation of all bounce back nodes. The distribution of interest can be realized by varying the number of catalyst particles only in $x-$direction, while it is kept quasi-homogeneous in the $y, z-$directions. Hence, the $x-$direction distribution is here treated as a tunable parameter of the morphological model in [1], with a large number of distributions (e.g. Gauss, Kronecker-delta, etc.) possibly realizable and testable. To find a link between the coefficients of the two considered distributions, we assume that the catalyst loading coefficient, α^{homo}, in homogeneous conditions is given. Conservation of the total number of catalyst particles yields, $\sum_{i=1}^{n_p} N_t \alpha^{exp} \exp(-\beta x_i) = \sum_{i=1}^{n_p} N_i^{homo} = n_p \alpha^{homo} N_t$, where the loading coefficient in the exponential distribution is $\alpha^{exp} = \alpha^{homo} \frac{n_p}{\sum_{i=1}^{n_p} \exp(-\beta x_i)}$. In general, a similar procedure can be followed to find a relation between α^{homo} and parameters for other desired distributions.

As mentioned above, for simplicity, x is assumed to be the direction of the main mass transport. In particular, at $x_{cl} = 0$ and $x_{cl} = 1$ we locate the gas diffusion/catalyst layer interface and the catalyst layer/polymeric membrane interface, respectively. In the following, results are often reported

in terms of the dimensionless coordinate $x_{cl} = x/l_{CL}$, where l_{CL} is the CL thickness. Homogeneous distribution can be considered as representative of conventional Pt distribution (see recent tomography data of catalyst layer presented in Ref. [47]). The primary goal of a pore-scale model is to provide a macroscopic counterpart with suitable parameters. Particularly, mass transport properties for the catalyst layer (i.e. tortuosity and permeability) are highly affected by micro-morphological parameters. Indeed, as shown in [1], the permeability is affected by carbon support clusterization size, catalyst distribution and Knudsen parameter (gas rarefaction level).

2.2. Three-dimensional macroscopic model of the membrane electrode assembly

In this section, we describe a three-dimensional macroscopic model of the membrane electrode assembly (MEA). This will be used for computing the flow field at the catalyst layer as well as the performance (i.e. the polarization curve) for different catalyst layer configurations. The three-dimensional model of a single MEA is presented in Fig. 2. Here, the anode and the cathode catalyst layers are considered as made by multiple sublayers with different Pt catalyst loads. In order to consider a smooth profile of Pt particle distribution (as in the previous section 2.1), a large number of sublayers is needed, and this is clearly unpractical for manufacturing purposes. For simplicity, we have considered the catalyst layer containing three separate sublayers with different discrete values of the catalyst load. Details on the spatial dimensions of the MEA compartments can be found in Table 2.

A three-dimensional, single-phase, isothermal model for HT-PEMFC is considered with a coupling of transport and electro-chemistry phenomena.

The following assumptions are made:

- The fluid flow is incompressible and laminar.
- The gas mixtures obey the ideal gas law.
- Water is present in both anode and cathode sides, however it is produced only at the cathode side.
- Water exists only in a gas phase.
- The membrane is assumed to be impermeable to all gases.
- Electrical resistance of connections between different compartments of MEA is negligible.

Hence, the above model describes two transport phenomena. The first is the steady-state transport of reactants and water within all compartments of a MEA (except for the membrane, which is considered as impermeable for fluids). The second one is the transport of charges which concerns gas diffusion and catalyst layers for electrons and catalyst layer and membrane for protons.

2.2.1. Electrochemical reactions

A hydrogen-rich fuel stream containing water is supplied to the anode channel, and partly goes through the GDL. At the anode CL hydrogen oxidation occurs according to the reaction:

$$H_2 \Rightarrow 2H^+ + 2e^-. \tag{1}$$

Electrons produced by this reaction migrate across the cell through the following elements: carbon support particles embedded in the anode catalyst layer, fibers of GDLs, current collector, external circuit, cathode catalyst layer. On the other hand, protons follow a shorter path, across the membrane from the anode towards the cathode catalyst layer. Here, we assume that water molecules are not involved in the proton transport.

Moreover, the local current density for the hydrogen oxidation reaction is expressed by a linearized concentration dependent Butler-Volmer expression (see for example [48]):

$$i_a = a_\nu i_{0,a}^{ref} \left(\frac{c_{H_2}}{c_{H_2}^{ref}} \right)^{0.5} \left(\frac{\alpha_a}{RT} F\eta \right), \tag{2}$$

where $i_{0,a}^{ref}, c_{H_2}, c_{H_2}^{ref}$ are the exchange current density, the local hydrogen and a hydrogen reference concentrations, respectively, with α being a reaction coefficient, T the temperature, F the Faraday, R the ideal gas constants and η a local overpotential. The effective surface area, a_ν, is defined as the ratio of the total active catalyst surface area to the total CL volume.

The cathode channel is fed by air. At the cathode, oxygen reacts with protons to form water as follows:

$$O_2 + 4H^+ + 4e^- \Rightarrow 2H_2O \tag{3}$$

A simplified Butler-Volmer expression can be considered, where the anodic term has been omitted, and a Tafel-equation (thus introducing a dependency on concentrations) can be used as a current density expression for the oxygen reduction reaction [48]:

$$i_c = -a_\nu i_{0,c}^{ref} \left(\frac{c_{O_2}}{c_{O_2}^{ref}} \right) \exp\left(\frac{\alpha_c}{RT} F\eta \right), \tag{4}$$

where $i_{0,a}^{ref}, c_{O_2},\ c_{O_2}^{ref}$ are the exchange current density, the local hydrogen concentration and an oxygen reference concentrations, respectively.

2.2.2. Governing equations

The global mass-transport process in HT-PEMFC takes place in three different media: the gas channels, gas diffusion layer, and catalyst layer. The electrolyte membrane is considered to be impermeable to all gases.

The following incompressible Navier-Stokes equations can be used to describe the fluid continuity and momentum transport of the laminar gas flow within channels at both anode and cathode sides:

$$\rho \mathbf{u} \cdot \nabla \mathbf{u} = \nabla \cdot \left[-pI + \mu(\nabla \mathbf{u} + \nabla \mathbf{u}^T) \right], \tag{5}$$

$$\rho \nabla \cdot \mathbf{u} = 0, \tag{6}$$

where $\rho, \mathbf{u}, p, \mu$ are density, velocity vector, pressure, dynamical viscosity, respectively.

To describe the gas flow within the GDL and CL porous media the Brinkman equations can be utilized [49]:

$$\frac{\rho}{\varepsilon}\left(\mathbf{u} \cdot \nabla \frac{\mathbf{u}}{\varepsilon}\right) = \nabla \cdot \left[-p\mathbf{I} + \frac{\mu}{\varepsilon}(\nabla \mathbf{u} + \nabla \mathbf{u}^T) - \frac{2\mu}{3\varepsilon}(\nabla \cdot \mathbf{u})\mathbf{I} \right], \\ - \left(\frac{\mu}{k} + \beta_r |\mathbf{u}| + S_m\right)\mathbf{u}, \tag{7}$$

$$\rho \nabla \cdot \mathbf{u} = S_m \tag{8}$$

where ε, k are two parameters of porous medium, namely porosity and permeability.

The mass source/sink term can be explicitly written as:

$$S_m = \begin{cases} -M_{H_2} \frac{i_a}{2F}, & \text{at} \quad \text{anode} \quad \text{CL} \\ M_{O_2} \frac{i_c}{4F} - M_{H_2O} \frac{i_c}{2F}, & \text{at} \quad \text{cathode} \quad \text{CL}. \end{cases} \tag{9}$$

The equation for the conservation of the chemical species in the channels is written using the Stefan-Maxwell equations [49] accounting for diffusion of hydrogen (H_2) and water (H_2O) at the anode side, as well as oxygen (O_2), water (H_2O) and nitrogen (N_2) at the cathode side:

$$\rho\mathbf{u}\cdot\nabla\omega_i = \nabla\cdot\left[\rho\varepsilon\omega_i\sum_i D_{ik}^{eff}\left(\frac{Mt}{M_k}\nabla\omega_i + \frac{\omega_k}{p}\left(\frac{M_{total}}{M_k}-1\right)\nabla p\right)\right] + S_{\omega_i}, \quad (10)$$

where ω_i is the mass fraction for $i-$th species, M is the molar mass, while D_{ik}^{eff} is the binary diffusion coefficient with M_{total} being:

$$M_{total} = \left(\sum_i \frac{\omega_i}{M_i}\right)^{-1}. \quad (11)$$

The source terms for all the species in (10) are:

$$S_{\omega_i} = \begin{cases} \frac{i_a}{2F}, & \text{for} \quad H_2 \quad \text{at} \quad \text{anode} \quad \text{CL} \\ \frac{i_c}{4F}, & \text{for} \quad O_2 \quad \text{at} \quad \text{cathode} \quad \text{CL} \\ \frac{i_c}{2F}, & \text{for} \quad H_2O \quad \text{at} \quad \text{cathode} \quad \text{CL}. \end{cases} \quad (12)$$

The Stefan-Maxwell (SM) model for diffusion is the most general approach for describing multicomponent mass transport. As opposed to Fick's model, it allows to reproduce typical diffusive effects of ternary mixtures, which are not present in binary diffusion, such as counter diffusion. In the limit of binary mixtures the Stefan-Maxwell model reduces to the Fick's model. In addition, the SM model has a more solid thermodynamic basis compared to the phenomenological formulation of Fick's equation, and it can be formulated for taking into account the effect of both external body forces and non-equilibrium behaviors of fluids such as rarefaction. The latter model has been included in a lattice Boltzmann solver by an author of this paper [51].

The transport of charges (electron and proton) may occur through the solid (i.e. a network of carbon support of catalyst and carbon fibers based gas diffusion layer) and the electrolyte (polymer ionomer linkage in catalyst layer and membrane) phases. Poisson equations are used to describe the transport of electrons within the solid-phase (subscript s) of GDL and CL, as well as in the electrolyte-phase (subscript e) within the CL and membrane accounting for ion transport. This yields:

$$\begin{aligned} \nabla \cdot \mathbf{i_s} &= S_\phi, \quad \mathbf{i_s} = -\sigma_s \cdot \nabla \phi_s, \\ \nabla \cdot \mathbf{i_e} &= -S_\phi, \quad \mathbf{i_e} = -\sigma_e \cdot \nabla \phi_e. \end{aligned} \tag{13}$$

Both equations are coupled through their current source/sink terms:

$$S_\phi = \begin{cases} i_a, & \text{at} \quad \text{anode} \quad \text{CL}, \\ i_c, & \text{at} \quad \text{cathode} \quad \text{CL}. \end{cases} \tag{14}$$

3. Simulation results and discussion

In this section the simulation results of both pore-scale and macroscopic models are presented. Moreover, how the catalyst particle redistribution within the porous CL affects the flow field and overall fuel cell performance is discussed.

The pore-scale simulations of a mass flow through porous electrodes have been performed using a BGK lattice Boltzmann method. The morphological model of a porous catalyst layer, as presented in [1], is used for the reconstruction. To mimic sink terms, i.e. electrochemical reaction areas, pressure boundary conditions are applied at the catalyst nodes. As mentioned in Section 2.1, catalyst nodes are assumed to be deposited on the surface of carbon

support agglomerates. Values of the imposed pressure (p) are assumed as a function of the distance from the membrane:

$$p = p_0 - x_{cl} \cdot \delta p, \tag{15}$$

with p_0 being the pressure at the inlet ($x_{cl} = 0$). Hence, the pressure gradient ∇p is kept at a constant value δp, and this provides the same reaction probability for all catalyst particles:

$$\nabla p = \frac{\partial p}{\partial x} = -\delta p. \tag{16}$$

Below, it is demonstrated that the choice of this boundary condition provides consistent results with the macroscopic model. A laminar flow regime can be achieved by imposing very small values of δp. Moreover, the effect of an impermeable (to fluids) membrane is accounted by the so-called bounce-back boundary conditions at the CL/membrane interface, whereas periodicity is enforced on lateral boundaries. More details on porous media, computational domain, and input LBM parameters are reported in Table 1. Notice that, the LBM input parameters and results are given in dimensionless units (lattice units $l.u.$, see, e.g., [50]).

The module *Batteries & Fuel Cells* by COMSOL® Multiphysics software package [52] has been utilized for performing all simulations of the macroscopic approach with the following parameters and conditions. The convergence criteria for all species and energy calculation residuals are set to 10^{-8}. In Table 3, we summarize physical properties of the gas mixture, fuel cell materials and operating conditions. The following initial and boundary conditions have been applied in this model. At the channel inlets the mass

fractions are specified, and outflow conditions are used at the channel outlets. Zero flux conditions are used for all other external boundaries. At the flow channel inlet boundaries, laminar inlet flow velocity profiles are specified, whereas a pressure is specified at the flow channel outlet boundaries. To model a multiple parallel channel configuration, symmetry boundary conditions are applied for the long sides of the GDLs and the porous electrodes. All other wall boundaries make use of no-slip conditions. The grid used for the catalyst layer discretization has been refined to accurately describe the expected local gradients, whereas a coarser grid was sufficient within the gas channels and gas diffusion layers. Additional details on the cell geometry are given in Table 2. The total number of degrees of freedom for this problem is 111.722.

3.1. Flow velocity results

The primary quantity of interest of both pore-scale and macroscopic simulations is the component of the flow velocity u along the main direction x. The main reason is that the gradient of the latter quantity dictates the pulling stress τ exerted on the phosphoric acid by gases. Specifically, the larger this stress the larger the force acting on phosphoric acid driving an undesired phosphoric acid flux (j_{PA}) through diffusion and capillary transport mechanisms. In other words, there is a direct relation between the fuel cell degradation caused by phosphoric acid losses from the membrane and the velocity gradient at $x_{cl} = 1$ (i.e. the CL/membrane interface):

$$j_{PA} \propto \tau_x = -\mu \left.\frac{\partial u}{\partial x}\right|_{x_{cl}=1}, \tag{17}$$

with μ being the dynamic viscosity of the fluid.

An optimal distribution of the catalyst inside the CL is expected to properly modulate the flow field in such a way that not only velocity, but also its gradient is equal to zero at the CL/membrane interface.

$$\begin{aligned} u\,|_{x_{cl}=1} &= 0; \\ \left.\frac{\partial u}{\partial x}\right|_{x_{cl}=1} &= 0; \\ j_{PA} \propto \tau_x = -\,\mu \left.\frac{\partial u}{\partial x}\right|_{x_{cl}=1} &= 0. \end{aligned} \tag{18}$$

This is believed to prevent phosphoric acid loss from the membrane and catalyst layer itself due to fluid stress and reagents crossover through membrane.

Below, we first consider the results of pore-scale simulations. In Fig. 3 the velocity profile along the flow direction is reported for the homogeneous catalyst particle distribution. In particular, the red curve with symbols represents the velocity component within the CL along the main flow direction (averaged over orthogonal planes). We found a significant mismatch of this profile compared to the following analytical expectation:

$$u_x = \frac{k\nabla p}{\mu}\alpha^{homo}(l_{CL} - x_{cl}), \tag{19}$$

with k being the permeability of a porous catalyst electrode.

The analytical expression (19) is based on the continuity equation for incompressible flow, periodicity of lateral walls and the assumption of homogeneous catalyst distribution. Several possible explanations of this mismatch have been analyzed. It was found that the permeability value is rather sensitive to the catalyst loading level, and it is a function of the porous medium length. The main reason of the observed behavior is that the activity of catalyst particles highly depends on their location. Indeed, as visible in Fig. 3 (curved

line), the flow field is quasi-constant (i.e. catalyst particles are less active) close to the GDL, whereas a sharp drop (high activity) is observed nearby the membrane area. In these pore-scale models, a difference between the imposed pressure at the catalyst and the average pressure of the surrounding flow indicates the level of activity. To check this, the profile of mean pressure (averaged over planes orthogonal to the main flow direction) has been reported in Fig. 4 (left top). The curved line indicates the result of pore-scale simulations, while the straight line is the imposed pressure. Clearly, the pressure difference considerably increases close to the membrane (see the plot in the left-bottom part of Fig. 4).

At a macroscopic level, the catalyst activity refers to the reaction current density, which is in turn function of the reagent concentration (c) and the local overpotential (η), as presented in Eq. (2). These quantities may change with the distance. The local overpotential of the porous electrode can be defined as

$$\eta(x) = \phi_s(x) - \phi_e(x) - \Delta\phi_{ref} - E_{th} \tag{20}$$

where ϕ_s and ϕ_e are the potentials in the solid and electrolyte phases, respectively, while $\Delta\phi_{ref}$ is the potential difference across the interface for a reference electrode (this is here constant, hence $\Delta\phi_{ref} = 0$). In the right-top part of Fig. 4, we report the electric and electrolyte potentials along the the central line $z = (h_{RIB} + h_{CH})/2$ on the orthogonal cut plane at $y = l_{CELL}/2$. The lower the local overpotential $\eta(x)$ the larger the current density of electrode, whose profile is shown in the right bottom part of Fig. 4. A contour map of the flow velocity (x-component only, obtained by the macroscopic model) on the MEA middle plane is depicted in Fig. 5 (a), while its profile

along the centerline of the above plane is shown in Fig. 5 (b). The latter results refer to an homogeneous catalyst particle distribution within the CL. For the sake of comparison with results from the pore-scale modeling, a magnification of the CL region is also reported in the inset of Fig. 5 (b). We stress that the two modeling approaches (i.e. pore-scale vs macroscopic model) adopt entirely different boundary conditions at the reaction sites. Hence, the qualitative agreement found can be assumed as a proof of the suitability of the chosen pressure boundary conditions.

As shown in Fig. 6, the velocity values vanish at the interface region for the two different catalyst distributions (homogeneous and exponential decay), however a completely different behavior of the velocity gradient (straight line) can be observed. In particular, a switch from the homogeneous to an exponential decay distribution of the catalyst particles leads to a reduction of the pulling stress over one order of magnitude (according to the pore-scale model) and about 67% (according to the macro-scale model). See also the Table 1. Results from the pore-scale simulation can be considered as an upper limit for macroscopic results due to a simplified treatment of the CL. In fact, as mentioned in Section 2.2, the CL is discretized by only three sub-layers with different values of catalyst particle load. In conclusion, the adoption of a CL with an exponential decay distribution of particles (from the gas diffusion layer towards the membrane) ensures the desired velocity gradient profile, which provides a considerable reduction of the fluid stress nearby the membrane. Consequently, in the near future, strategies for improving HT-PEMFC durability may be based for the optimal design of the catalyst distribution. Additional details on how the flow field is affected by

the catalyst distribution with exponential decay towards the membrane are provided in Fig. 7. Changes in terms of both the main flow rate and fluid flow streamlines are observed. As it can be seen in the upper-left part of Fig. 7, when a homogeneous catalyst distribution is adopted in the CL, a considerable number of flow streamlines with non-negligible velocity magnitude can be observed at the CL/membrane interface. On the other hand, much fewer streamlines are able to reach the same interface when an exponential decay distribution of the catalyst is adopted in the CL. In fact, in the upper-right part of Fig. 7, we report the flow streamlines for the exponential decay distribution stemming from the same points as in the upper-left plot of Fig. 7. As a result, the latter distribution ensures a significant reduction of the pulling stress on the PA contained within the polymeric membrane.

The advantage of having the aforementioned exponential decay distribution of the catalyst particles is twofold. Firstly, the degradation phenomena due to phosphoric acid loss and crossover of gases through membrane are mitigated. Secondly, owing to improved flow field an increase of the threshold for mass transport overpotential at high current density is expected, which leads to an increase of the overall cell efficiency (peak value of performance).

3.2. Single MEA performance simulation

Fig. 8 displays the simulated HTPEMFC overall performance in terms of the polarization curve corresponding to the base case in Table 3. Three different distributions of the Pt catalyst particles inside the CL both at the anode and cathode side were considered as listed below:

(c1) homogeneous;

(c2) exponential decay towards the polymeric membrane;

(c3) exponential increase towards the polymeric membrane.

The quasi-homogeneous distribution of catalyst particles is assumed as representative of a conventional CL, while an exponential decay is suggested to be an optimal distribution for reducing the phosphoric acid losses caused by the pulling stress of reactants flow (see previous Section 2.1). In the third case, we expect detrimental performances in terms of membrane degradation (i.e. PA loss), as experimentally observed in [2] where catalyst particles are mostly found nearby the CL/Membrane at the end of the cell lifetime. However, a better cell performance is also expected due to the vicinity of reaction layers to the membrane leading to enhanced ionic conductivity. We also stress that, pore-scale analysis of the latter exponential increase distribution case is beyond the scope of this work, where we are mainly focused on a mitigation strategy for the PA degradation phenomenon. As mentioned before, for the sake of simplicity, a minimal number of discrete values for the Pt catalyst loadings has been used, and this only allows to carry out a qualitative analysis.

The polarization curves presented in Fig. 8 show a typical PEMFC behavior. We stress that here we do not take into account one of the important parts of the polarization curve, namely the mass transport overpotential in high current density region. Hence, the polarization curves can be divided into two regions. The first one is the low current density region ($j \in (0, 0.1)\ A/m^2$), where approximately the same sharp voltage drop can be observed in the three cases. This drop is known to be due to activation losses (kinetics). At the moderate current density values, Ohmic losses determine

a linear decrease of the overall cell potential. Those losses are mainly due to both the ionic and electronic resistances. The former one is generated within the polymeric membrane and ionomer of the CL, while the latter within the catalyst carbon support (carbon black) and the GDL fibers. Note that the electrical resistance of gas channels has been considered as negligible. The polarization curves show different decay slopes for the three analyzed cases, where the steepest slope was observed for the case (c2), while the less steep one for the case (c3) (see Fig. 8). This could be explained as follows. In the case (c2), the majority of H^+ ions is produced in the CL sublayer, which is located far away from the polymeric membrane. Thus, H^+ ions have to travel longer to reach the membrane compared to the cases (c1) and (c3), which consequently increases the average CL ionic resistance. On the other hand, in (c2), on average the pathway followed by the produced electrons is shorter, and this obviously decreases the CL electronic resistance. Owing to the fact that conductivity of carbon black is much higher than conductivity of the electrolyte, $\sigma_s \gg \sigma_e$ (see also Table 3), an overall increase in the Ohmic voltage drop is observed. This led to 9.3% difference in performance at high current density when using exponential decay catalyst distribution (compared to homogeneous catalyst case). Finally, it should be noted that during cell operation a dynamic change of the catalyst particle distribution has been experimentally observed [2]. Even starting with quasi-homogeneous distribution of Pt catalyst in a virgin fuel cell, a redistribution of catalyst towards the membrane is experienced. Namely, at the end of the cell life-time a significant amount of catalyst particles has been detected in the neighborhood of the polymeric membrane. This fact further justifies our suggestion

on catalyst particle distribution inside the CL of virgin HTPEMFC.

4. Conclusions

This work has investigated i) how the distribution of catalyst particles within the CL of a fuel cell affects the flow field, and ii) how this can be used as a mitigation strategy against phosphoric acid loss and crossover of reagents through the cell membrane.

To this end, a pore-scale model of the fluid flow through the cell CL shows that a switch of the catalyst particle distribution from the traditional homogeneous one in favor of an exponential decay profile reduces the pulling stress over an order of magnitude. This is twofold advantageous: first, it reduces the cell degradation due to phosphoric acid loss and crossover of gases through the membrane. Second, an enhancement of the overall fuel cell performance is expected owing to an augmented flow rate which, in turn, increases the threshold for mass transport overpotential at high current density.

In addition, a simplified macroscopic model (performed over a single MEA) suggested that the proposed mitigation strategy is able to significantly reduce phosphoric acid loss due to pulling stress (up to 67% at the price of only 9.3% reduction in efficiency at high current densities.)

It is well known that one of the main trends to improve overall performance of HT PBI-based PA-doped PEMFC is to reduce ionic resistance by increasing PA doping level. To this respect, it is worth emphasizing that the proposed confinement strategy could lead to the use of membranes with increased amount of PA in the near future, as far as suitable materials be-

come available.Our suggestion of adopting an exponential decay distribution for the catalyst particles within the CL may be further supported by recent experimental data on the dynamic evolution of CL structure during cell operation. In fact, it has been proved that a large number of the catalyst particles migrates towards a narrow area near the polymeric membrane at the end the cell life-time [2].

HT-PEMFC operating at elevated temperature is definitively a promising technology, due to many reasons, such as enhanced electrochemical kinetics, simplified water management and cooling, and enhanced carbon monoxide tolerance. However, durability remains challenging. There are two main degradation phenomena which are responsible for these issues: agglomeration of catalyst particles and phosphoric acid loss from the membrane.

Deeper insights of those degradation phenomena may come from multi-scale modeling. In particular, pore-scale modeling of transport mechanisms of gases inside different compartments of fuel cells can reveal certainly a powerful tool towards a satisfactory accomplishment of this goal. The latter aspect is important because it allows to design possible new mitigation strategies for enhancing fuel cell durability in the near future.

Acknowledgements

Authors would like to acknowledge the support of the European project ARTEMIS "Automotive Range extender with high TEMperature Improved pemfc meas and Stacks" 2012-2015 (Grant Agreement No.303482). Authors would like to thank Dr. Deborah Jones and Yannig Nedellec, Université Montpellier 2 and Dr. Arnaud Morin, LITEN, CEA for useful discussions

and comments.

[1] U. R. Salomov, E. Chiavazzo, P.Asinari, Pore-scale modeling of fluid flow through gas diffusion and catalyst layers for high temperature proton exchange membrane (HT-PEM) fuel cells, Computers & Mathematics with Applications 67 (2014) 393-411.

[2] Y. Oono, A. Sounai, M. Hori, Long-term cell degradation mechanism in high-temperature proton exchange membrane fuel cells, Journal of Power Sources 210 (2012) 366-373.

[3] A.B. LaConti, M. Hamdan, R.C. McDonald, in: W. Vielstich, H. Gasteiger, A. Lamm (Eds.), Handbook of Fuel Cells Fundamentals, Technology and Applications, vol. 3, John Wiley & Sons, New York, 2003.

[4] M.F. Mathias, R. Makharia, H.A. Gasteiger, J.J. Conley, T.J. Fuller, C.J. Gittleman, S.S. Kocha, D.P. Miller, C.K. Mittelsteadt, T. Xie, S.G. Yan, P.T. Yu, Two fuel cell cars in every garage?, Electrochem. Soc. Interface 14 (2005) 24-36.

[5] Q. Li, J.O. Jensen, R.F. Savinell, N.J. Bjerrum, High temperature proton exchange membranes based on polybenzimidazoles for fuel cells, Prog. Polym. Sci. 34 (2009) 449-477.

[6] A.R. Korsgaard, R. Refshauge, M.P. Nielsen, M. Bang, S.K. Kær, Experimental characterization and modeling of commercial polybenzimidazole-based MEA performance, Journal of Power Sources 162 (2006) 239.

[7] Y.-L. Ma, J.S. Wainright, M.H. Litt, R.F. Savinell, Conductivity of PBI membranes for high-temperature polymer electrolyte fuel cells, Journal of The Electrochemical Society 151 (2004) A8-A16.

[8] J.A. Asensio, S. Bòrros, P. Gòmez-Romero, Enhanced conductivity in polyanion-containing PBIs. Improved materials for PEM membranes and Fuel Cells, Electrochemistry Communications 5 (2003) 967-972.

[9] J.R.P. Jayakody, S.H. Chung, L. Durantio, H. Zhang, L. Xiao, B.C. Benicewicz, S.G. Greenbaum, NMR Studies of Mass Transport in High-Acid-Content Fuel Cell Membranes Based on Phosphoric Acid and Polybenzimidazole, Journal of The Electrochemical Society 154 (2007) B242-B246.

[10] J. Parrondo, F. Mijangos, B. Rambabu, Platinum/tin oxide/carbon cathode catalyst for high temperature PEM fuel cell, Journal of Power Sources 195 (2010) 3977-3983.

[11] J. Lobato, P. Cañizares, M.A. Rodrigo, F.J. Pinar, D. Ùbeda, Study of flow channel geometry using current distribution measurement in a high temperature polymer electrolyte membrane fuel cell, Journal of Power Sources 196 (2011) 4209-4217.

[12] J. Zhang, Y. Tang, C. Song, J. Zhang, Polybenzimidazole-membrane-based PEM fuel cell in the temperature range of 120-200 ^{o}C, Journal of Power Sources 172 (2007) 163-171.

[13] A. Sounai, K. Sakai, Proceedings of the 13th Fuel Cell FCDIC Symposium (2006) 125.

[14] J. Baurmeister, T. Kohno, Proceedings of the 13th Fuel Cell FCDIC Symposium (2006) 122.

[15] T.J. Schmidt, J. Baurmeister, Properties of high-temperature PEFC Celtec-P 1000 MEAs in start/stop operation mode, Journal of Power Sources 176 (2008) 428-434.

[16] R.A. Silva, T. Hashimoto, G.E. Thompson, C.M. Rangel, Characterization of MEA degradation for an open air cathode PEM fuel cell, Int. J. Hydrogen Energy 37 (2012) 7299-7308.

[17] A. Loselevich, A.A. Kornyshev, W. Lehnert, Degradation of solid oxide fuel cell anodes due to sintering of metal particles, Journal of The Electrochemical Society 144 (1997) 3010-3030.

[18] S. Ma, Q. Chen, F.H. Jøgensen, P.C. Stein, E.M. Skou, ^{19}F NMR studies of Nafion ionomer adsorption on PEMFC catalysts and supporting carbons, Solid State Ion 178 (2007) 1568-1578.

[19] T.J. Schmidt. Durability and degradation in high-temperature polymer electrolyte fuel cells, ECS Transactions 1(8) (2006) 19-31.

[20] S. Yu, L. Xiao, B.C. Benicewicz, Durability Studies of PBI-based High Temperature PEMFCs, Fuel Cells 8 (2008) 165-174.

[21] A.Z. Weber, Gas-Crossover and Membrane-Pinhole Effects in Polymer-Electrolyte Fuel Cells, Journal of The Electrochemical Society 155(6) (2008) B521-B531.

[22] W. Liu, K. Ruth, and G. Rusch, Membrane durability in PEM fuel cells, J. New Mater. Electrochem. Syst. 4 (2001) 227-32.

[23] M. Pianca, E. Barchiesi, G. Esposto, and S. Radice, End groups in fluoropolymers, J. Fluorine Chem. 95 (1999) 71-84.

[24] Q. Guo, P.N. Pintauro, H. Tang, S. O'Connor, Sulfonated and crosslinked polyphosphazene-based proton-exchange membranes, J. Membrane Science 154 (1999) 175-81.

[25] S. Bose, T. Kuila, T.X.H. Nguyen, N.H. Kim, Kin-tak Lau, J.H. Lee, Polymer membranes for high temperature proton exchange membrane fuel cell: Recent advances and challenges, Progress in Polymer Science 36 (2011) 813-843.

[26] F.N. Buchi, B. Gupta, O. Haas, G.G. Scherer, Study of radiation grafted FEP-G-polystyrene membranes as polymer electrolytes in fuel cells, Electrochim. Acta 40 (1995) 345-53.

[27] J. Xie, D.L. Wood, D.M. Wayne, T.A. Zawodzinski, P. Atanassov, R.L. Borup, Durability of PEFCs at high humidity conditions, Journal of The Electrochemical Society 152 (2005) A104-A113.

[28] S. Kundu, M.W. Fowler, L.C. Simon, R. Abouatallah, N. Beydokhti, Degradation analysis and modeling of reinforced catalyst coated membranes operated under OCV conditions, Journal of Power Sources 183 (2008) 619-628.

[29] M. Aoki, H. Uchida, M. Watanabe, Decomposition Mechanism of Perfluorosulfonic Acid Electrolyte in Polymer Electrolyte Fuel Cells, Electrochemistry Communications 8 (2006) 1509-1513.

[30] M.W. Fowler, R.F. Mann, J.C. Amphlett, B.A. Peppley, P.R. Roberge, Incorporation of voltage degradation into a generalised steady state electrochemical model for a PEM fuel cell, Journal of Power Sources 106 (2002) 274-283.

[31] K. Teranishi, K. Kawata, S. Tsushima, S. Hirai, Degradation mechanism of PEMFC under open circuit operation, Electrochem. Solid-State Lett. 9 (2006) 475-477.

[32] A.A. Franco, and M. Gerard, Multiscale Model of Carbon Corrosion in a PEFC: Coupling with Electrocatalysis and Impact on Performance Degradation, Journal of The Electrochemical Society 155(4) (2008) B367-B384.

[33] K. Malek and A.A. Franco, Microstructure-Based Modeling of Aging Mechanisms in Catalyst Layers of Polymer Electrolyte Fuel Cells, J. Phys. Chemistry B 115 (2011) 8088-8101.

[34] Y. Shao-Horn, W.C. Sheng, S. Chen, P.J. Ferreira, E.F. Holby, and D. Morgan, Instability of supported platinum nanoparticles in low- temperature fuel cells, Topics in Catalysis 46 (2007) 285-305.

[35] R.M. Darling, and J.P. Meyers, Kinetic Model of Platinum Dissolution, Journal of The Electrochemical Society 150 (2003) A1523-A1527.

[36] H. Wendt, T. Brenscheidt, A. Fischer, Optimisation and modelling of fuel cell electrodes with emphasis upon catalyst utilization, ageing phenomena and ageing prevention, Phil. Trans Royal Soc. Lond A 354 (1996) 1-15.

[37] R.M. Darling, and J.P. Meyers, Mathematical Model of Platinum Movement in PEM Fuel Cells, Journal of The Electrochemical Society 152 (2005) A242-A247.

[38] E.F. Holbya, and D. Morgan, Application of Pt Nanoparticle Dissolution and Oxidation Modeling to Understanding Degradation in PEM Fuel Cells, Journal of The Electrochemical Society 159(5) (2012) B578-B591.

[39] K. Kinoshita, J.A.S. Bett, Potentiodynamic analysis of surface oxides on carbon blacks, Carbon 11 (1973) 403-411.

[40] P.L. Antonucci, F. Romeo, M. Minutoli, E. Alderucci, N. Giordano, Electrochemical corrosion behavior of carbon black in phosphoric acid, Carbon 26 (1988) 197-203.

[41] P. Stonehart, D. Wheeler, in: B.E. Conway, C.G. Vayenas, R.E. White, M.E. Gamboa-Adelco (Eds.), Modern Aspects of Electrochemistry, vol. 38, Kluwer Academic Publishers, New York, 2005 (Chapter 4).

[42] A.D. Modestov, M.R. Tarasevich, V.Ya. Filimonov, N.M. Zagudaeva, Degradation of high temperature MEA with PBI-H_3PO_4 membrane in a life test, Electrochimica Acta 54 (2009) 7121-7127.

[43] P. Stonehart, Carbon substrates for phosphoric acid fuel cell cathodes, Carbon 22 (1984) 423-431.

[44] C.A. Reiser, L. Bregoli, T.W. Patterson, J.S. Yi, D. Yang, M.L. Perry, and T.D. Jarvi, A Reverse-Current Decay Mechanism for Fuel Cells, Electrochem. Solid-State Lett. 8 (2005) A273-A276.

[45] J.P. Meyers, and R.M. Darling, Model of Carbon Corrosion in PEM Fuel Cells, Journal of The Electrochemical Society 153(8) (2006) A1432-A1442.

[46] T. Sousa, M. Mamlouk, K. Scott, A dynamic non-isothermal model of a laboratory intermediate temperature fuel cell using PBI doped phosphoric acid membranes, Int. J. Hydrogen energy 35 (2010) 12065-12080.

[47] S. Thiele, T. Fürstenhaupt, D. Banham, T. Hutzenlaub, V. Birss, Ch. Ziegler, R. Zengerle, Multiscale tomography of nanoporous carbon-supported noble metal catalyst layers, Journal of Power Sources 228 (2013) 185-192.

[48] E. U. Ubong, Z. Shi, and X. Wang, Three-Dimensional Modeling and Experimental Study of a High Temperature PBI-Based PEM Fuel Cell, Journal of The Electrochemical Society 156(10) (2009) B1276-B1282.

[49] D.F. Cheddie, N.D.H. Munroe, Three dimensional modeling of high temperature PEM fuel cells, Journal of Power Sources 160 (2006) 215-223.

[50] S. Succi, The lattice Boltzmann equation for fluid dynamics and beyond, 2nd ed. Oxford University Press, New York, 2001.

[51] P. Asinari, Lattice Boltzmann scheme for mixture modeling: analysis of the continuum diffusion regimes recovering Maxwell-Stefan model and

incompressible Navier-Stokes equations, Physical Review E 80 (2009) 056701.

[52] Batteries & Fuel Cells, For Simulating Batteries and Fuel Cell Design and Operation, http://www.comsol.com/batteries-fuel-cells-module

List of Tables

Table 1: Input parameters of the pore-scale model and the predicted velocity gradient at the CL/Membrane interface. Parameters and outcomes of the lattice Boltzmann method are reported in dimensionless units (i.e. lattice units *l.u.*, see [50])

Name	Homogeneous	Exponential decay
Model geometrical parameters		
Considered domain size, L	30 μm	30 μm
Average size of clusters, L_{av}	1.5 μm	1.5 μm
Catalyst loading coefficient, α	0.1	0.6
Lattice Boltzmann method parameters		
Relaxation parameter, τ_{LB}	1.1 $l.u.$	1.1 $l.u.$
Lattice viscosity, ν	0.136364 $l.u.$	0.136364 $l.u.$
Pressure difference, δp	3.0×10^{-4} $l.u.$	3.0×10^{-4} $l.u.$
Domain size, N	$256 \times 256 \times 256$	$256 \times 256 \times 256$
Simulation results		
Pore-scale model		
velocity gradient	1.859×10^{-3} $l.u.$	0.091×10^{-3} $l.u.$
Macroscopic model		
velocity gradient	1.453×10^{2} $[1/s]$	0.871×10^{2} $[1/s]$

Table 2: Geometrical parameters used in the macroscopic model of a single MEA. See also the Fig. 2.

Parameter	Value	Units
Cell length, l_{CELL}	20.0	mm
Channel thickness, l_{CH}	1.0	mm
Channel height, h_{CH}	0.7874	mm
Rib height, h_{RIB}	0.90932	mm
GDL thickness, l_{GDL}	0.380	mm
CL thickness, l_{CL}	50.0	μm
Membrane thickness, l_{MEM}	100.0	μm

Table 3: Physical parameters and operating conditions.

Parameter	Value	Units
Porous media parameters		
GDL porosity, ε_{GDL}	0.4	
CL porosity, ε_{CL}	0.3	
GDL permeability, k_{GDL}	1.0×10^{-11}	m^2
CL permeability, k_{CL}	2.0×10^{-12}	m^2
Fluid flow parameters		
Inlet H_2 mass fraction (anode), ω_{H_2}	0.743	
Inlet H_2O mass fraction (cathode), ω_{H_2O}	0.023	
Inlet O_2 mass fraction (cathode), ω_{O_2}	0.228	
Anode inlet flow velocity, u_{in}^a	0.2	m/s
Cathode inlet flow velocity, u_{in}^c	0.5	m/s
Anode mixture viscosity, μ^a	1.19×10^{-5}	Pa·s
Cathode mixture viscosity, μ^c	2.46×10^{-5}	Pa·s
Hydrogen molar mass, M_{H_2}	0.002	kg/mol
Nitrogen molar mass, M_{N_2}	0.028	kg/mol
Water molar mass, M_{H_2O}	0.018	kg/mol
Oxygen molar mass, M_{O_2}	0.032	kg/mol
$H_2 - H_2O$ binary diffusion coefficient	1.81×10^{-4}	m^2/s
$N_2 - H_2O$ binary diffusion coefficient	0.51×10^{-4}	m^2/s
$O_2 - N_2$ binary diffusion coefficient	0.47×10^{-4}	m^2/s
$O_2 - H_2O$ binary diffusion coefficient	0.55×10^{-4}	m^2/s
Oxygen reference concentration, $c_{O_2}^{ref}$	40.88	mol/m^3
Hydrogen reference concentration, $c_{H_2}^{ref}$	40.88	mol/m^3
Electric parameters		
GDL electric conductivity, σ_s	222	S/m
Membrane conductivity, σ_e	9.825	S/m
Exchange current density (anode), $i_{0,a}^{ref}$	1.0×10^5	A/m^2
Exchange current density (cathode), $i_{0,c}^{ref}$	1.0	A/m^2
Operating conditions		
Cell temperature, T	453.15	K
Reference pressure, P	101	kPa
Cell voltage, V_0	0.9	V

Table 4: Results of the macroscopic model for three different catalyst loading distributions.

Homogeneous	Exponential decay	Exponential increase
The effective surface area, a_ν for the anode catalyst sub-layers, [1/m]		
1.0×10^4	2.0×10^4	0.27×10^4
1.0×10^4	0.73×10^4	0.73×10^4
1.0×10^4	0.27×10^4	2.0×10^4
The effective surface area, a_ν for cathode catalyst sub-layers, [1/m]		
1.0×10^4	2.0×10^4	0.27×10^4
1.0×10^4	0.73×10^4	0.73×10^4
1.0×10^4	0.27×10^4	2.0×10^4
Cell voltage at $j = 0.6\ A/m^2$ current density, [V]		
0.495	0.447	0.522

List of Figures

(a)

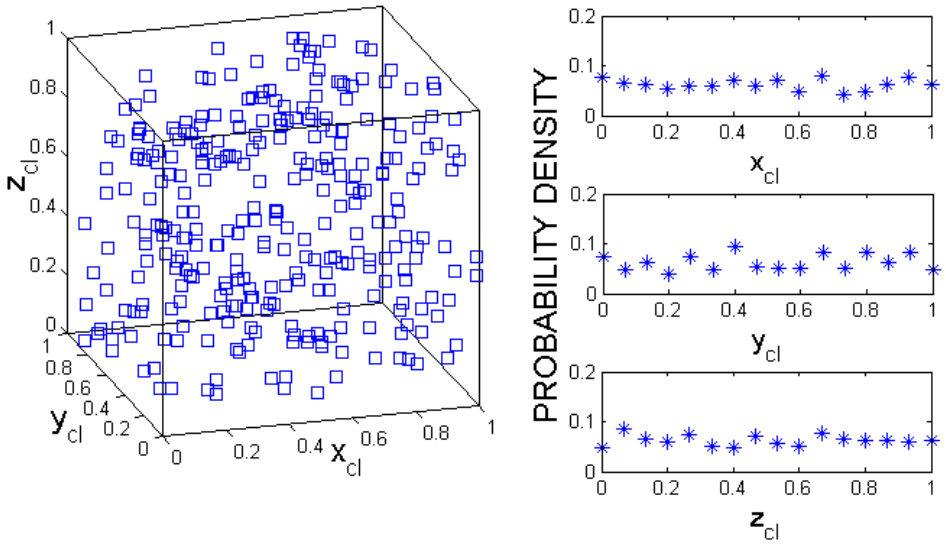

(b)

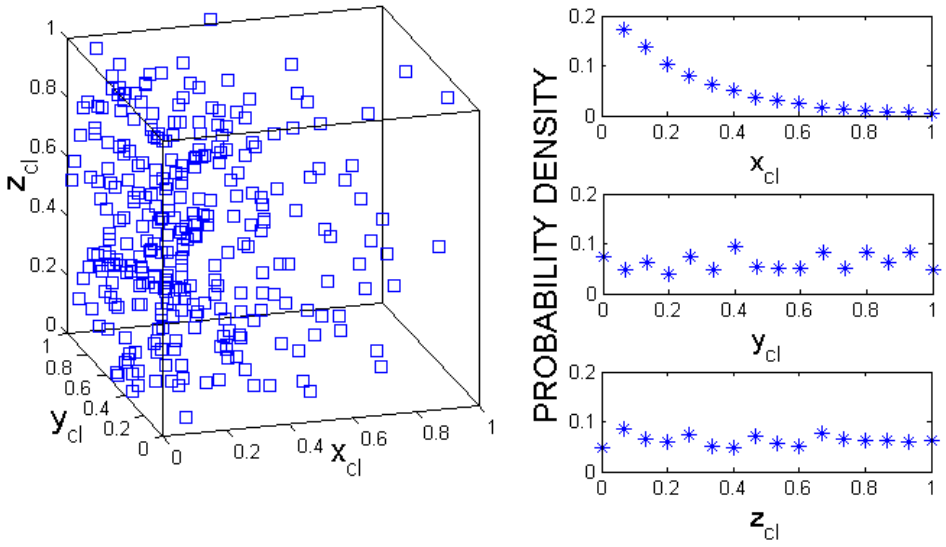

Figure 1: Left-hand side: Two representative cubic configurations of the CL with (a) homogeneous and (b) exponential decay catalyst particle distributions. Right-hand side: Probability distribution of catalyst particles along $x, y, z-$directions. Plots are reported in terms of the following dimensionless coordinates: $x_{cl} = x/l_{CL}$, $y_{cl} = y/l_{CL}$ and $z_{cl} = z/l_{CL}$.

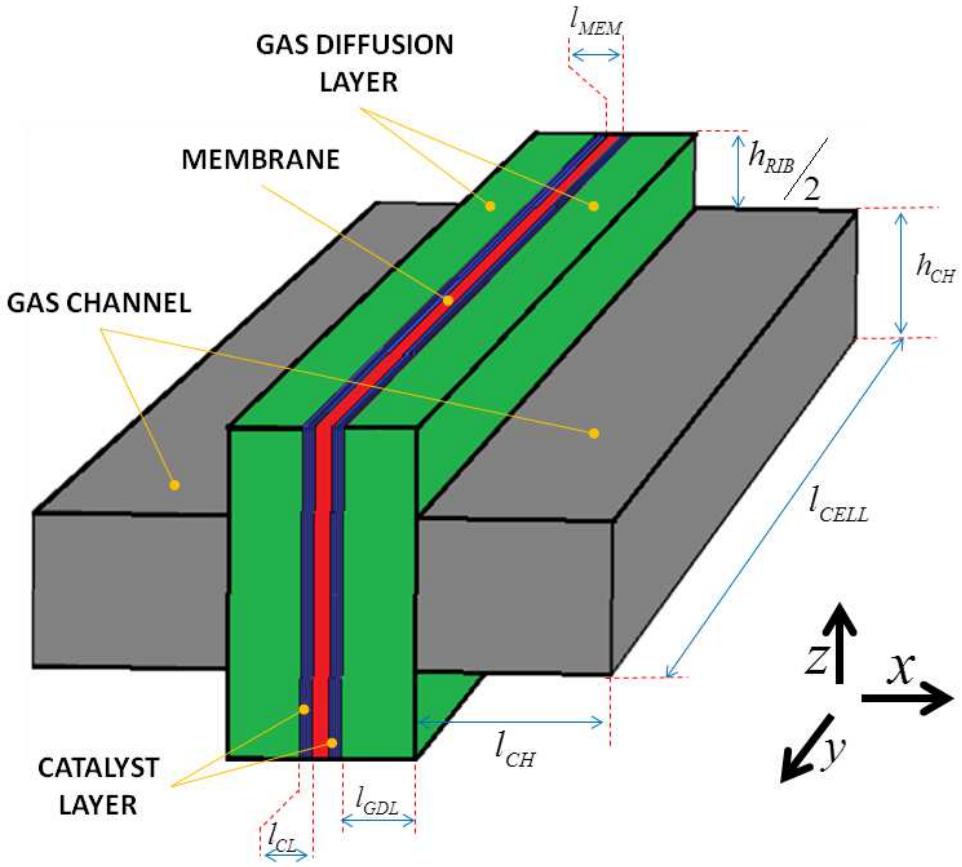

Figure 2: Single MEA geometry with the compartment names.

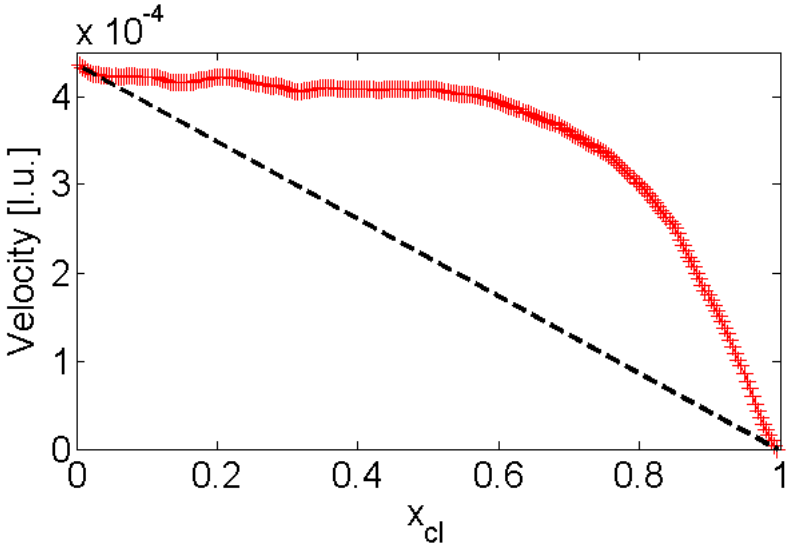

Figure 3: Profile of the x-component velocity averaged over the plane orthogonal to main flow direction (x). Symbols represent the result of pore-scale simulations for the homogeneous catalyst particle distribution. The straight line is the theoretical prediction. The abscissa indicates the dimensionless spatial coordinate $x_{cl} = x/l_{CL}$ across the CL, where the interface GDL/CL is located at $x_{cl} = 0$, while the interface CL/membrane is at $x_{cl} = 1$.

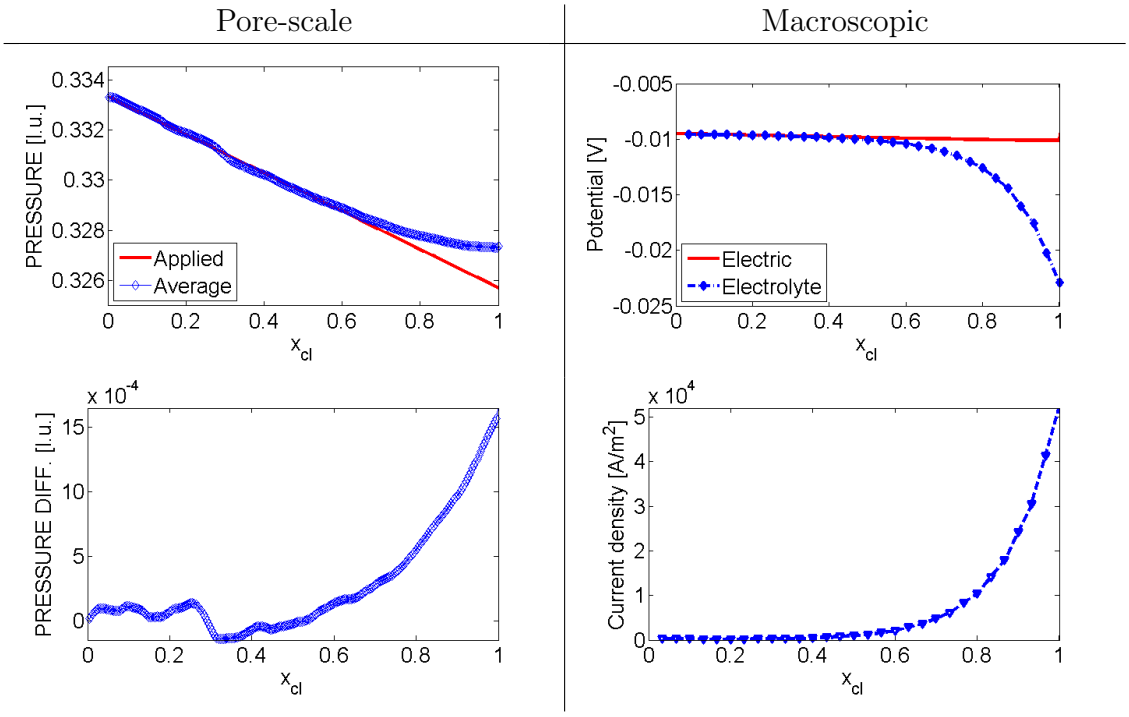

Figure 4: Left: Results of pore-scale simulations for $\delta p = 3.0 \times 10^{-4}$ $l.u.$ Right: Results of macroscopic model simulations with $V_{cell} = 0.6V$. Left-top: Average flow pressure (curved line) and imposed pressure at the catalyst nodes (straight line as dictated by (15)). Left-bottom: Difference of the above two pressures. Right-top: Electric and electrolyte potentials across the catalyst layer. Right-bottom: Electrode reaction current density inside the catalyst layer. Abscissas indicate the dimensionless spatial coordinate $x_{cl} = x/l_{CL}$ across the CL, where the interface GDL/CL is located at $x_{cl} = 0$, while the interface CL/membrane is at $x_{cl} = 1$.

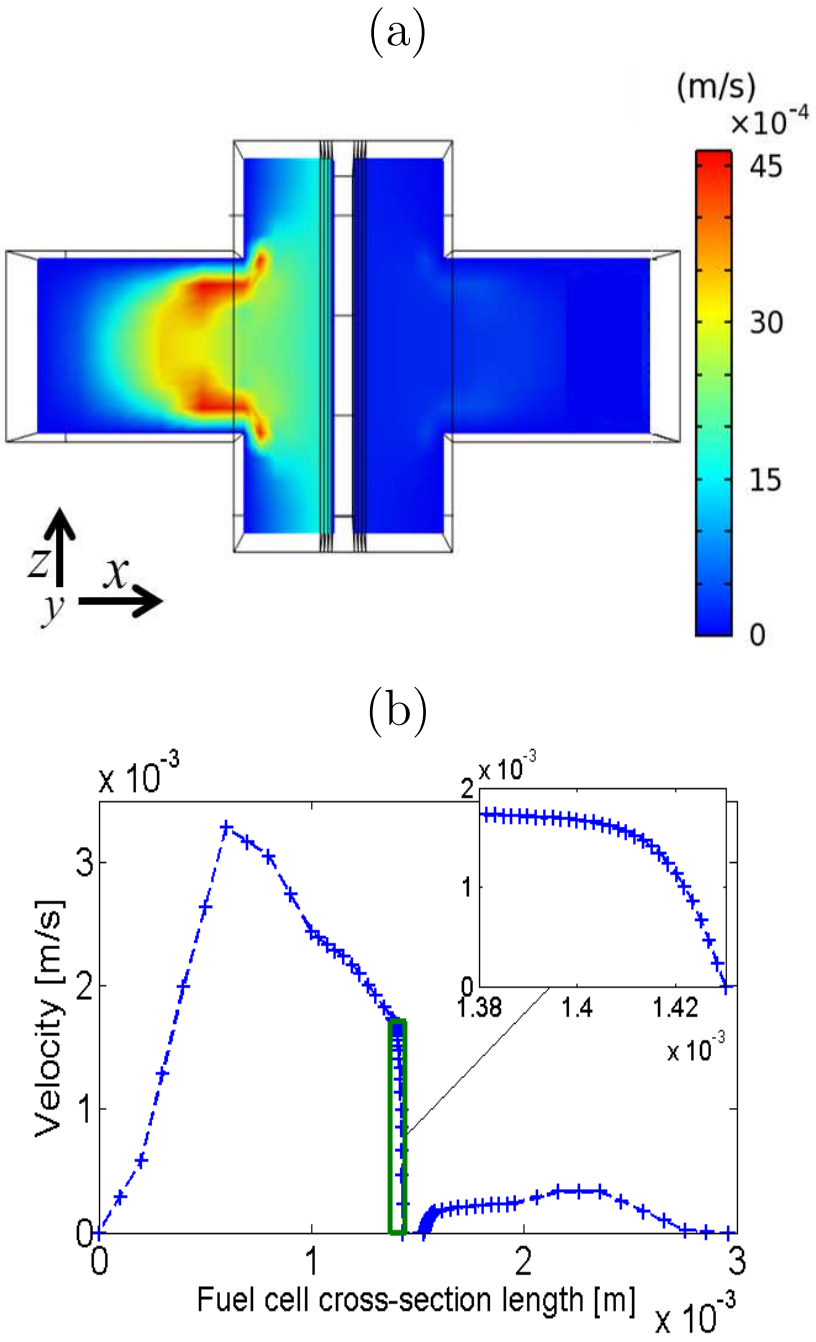

Figure 5: $x-$component velocity as derived by the macroscopic model at $V_{cell} = 0.6V$ with homogeneous catalyst loading: (a) on the middle plane of the MEA ($y = l_{CELL}/2$); (b) along the center line ($z = (h_{RIB} + h_{CH})/2$) of the above plane (see also Fig. 2). Inset: zoom of the velocity profile within the CL.

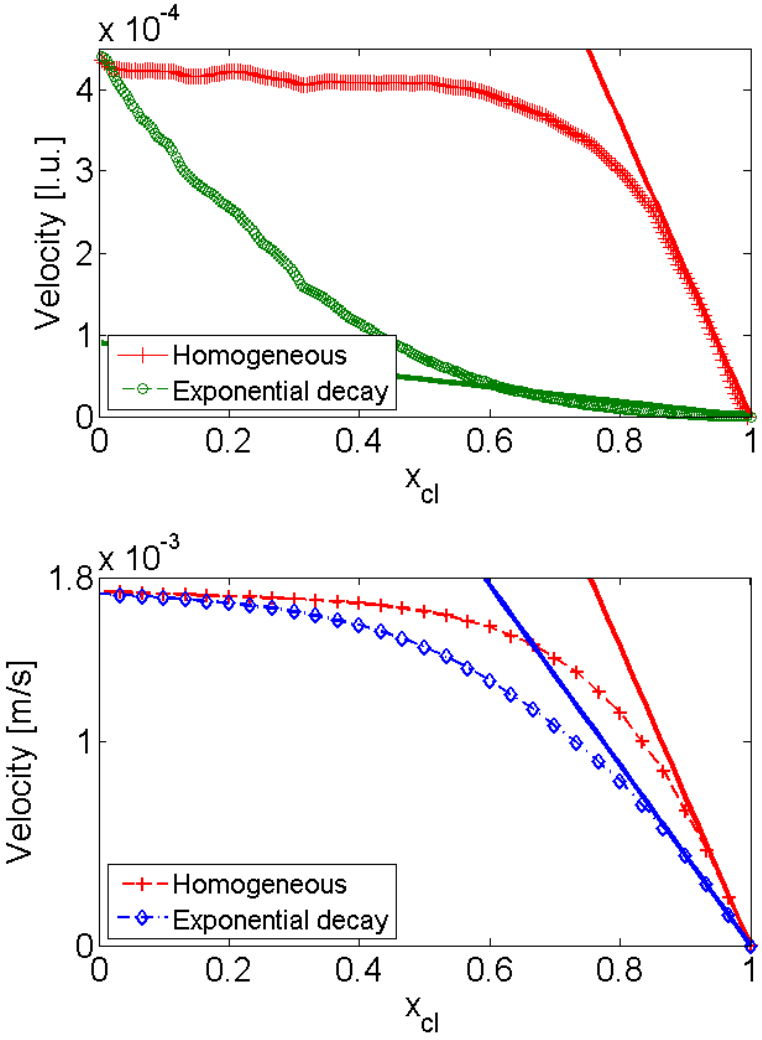

Figure 6: Velocity profiles corresponding to homogeneous and exponential decay catalyst particle distributions. Top: results of the pore-scale model with $\delta p = 3.0 \times 10^{-4}$ $l.u.$ Bottom: results of the macroscopic model with a current density $j = 0.6A/m^2$. Slopes of those profiles are also reported by straight lines.

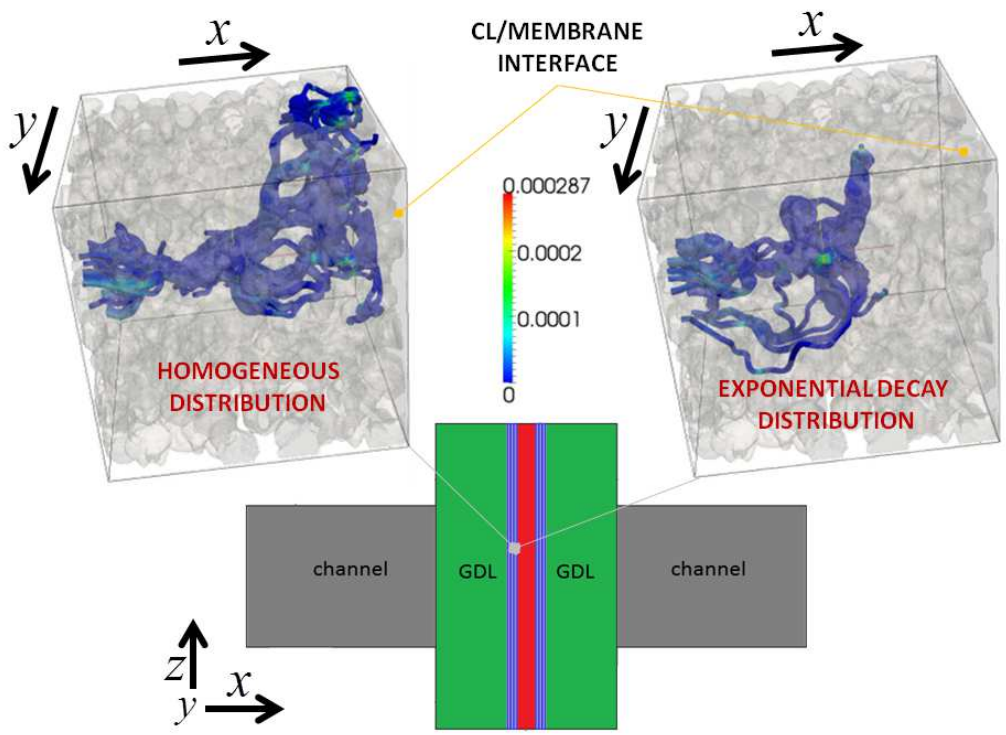

Figure 7: A cubic representative configuration of the CL of a HT-PEM fuel cell (bottom) is reconstructed by the method proposed in [1]. Fluid flow streamlines through the reconstructed CL porous medium (semi-transparent) corresponding to homogeneous distribution (upper-left) and exponential decay profile (upper-right). Streamline colors indicate the velocity magnitude in dimensionless lattice Boltzmann units.

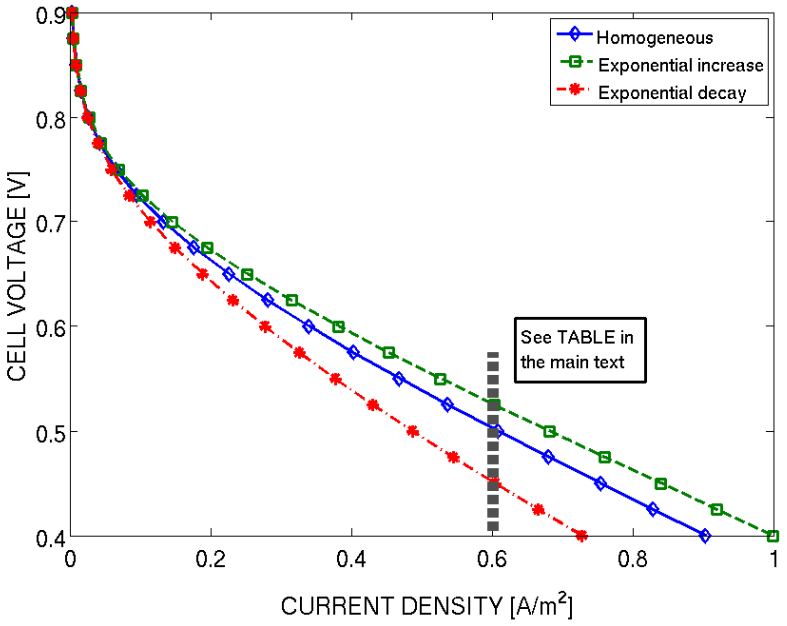

Figure 8: Polarization curves resulting from three different configurations of the catalyst particles distribution. The values of cell voltage at a current density of $j = 0.6\ A/m^2$ are presented in Table 4.